AITA
ARTIFICIAL INTELLIGENCE
THEORY AND APPLICATIONS

■ REVIEW ARTICLE

Modern Computer Tomography with Artificial Intelligence and Deep Learning Applications

Coşkun Deniz [a †]

[a]Department of Electrical and Electronics Engineering, Aydin Adnan Menderes University, Aydın, Türkiye
[†] cdeniz@adu.edu.tr,corresponding author

RECEIVED JUNE 20, 2023
ACCEPTED AUGUST 31, 2023

CITATION Deniz, C. (2023). Modern computer tomography with artificial intelligence and deep learning applications. *Artificial Intelligence Theory and Applications, 3*(2), 123-136.

Abstract

X-ray computed tomography (CT) aims production of 2-dimensional mass-density (or X-ray attenuation coefficient) maps of the sliced interior body by using directed X-rays through it to construct 3D CT images from the collection of these sliced 2D maps. Since the CT scan provides us with the interior structure of the body without any cut or physical damage, it is indispensable in our modern medical applications. However, since the X-rays involve ionizing radiation, it is dangerous for living organisms and it brings about the ALARA (as low as reasonably achievable) principle in medical applications emphasizing as high-quality CT images (with the highest possible resolution) as possible by using as little X-ray exposure of the body under scan as possible. This challenging task along with the correct interpretation of these CT images to lead a correct diagnosis and treatment plan brings about designing various fan geometries, scanning styles, and advanced image reconstruction techniques in the evolution of X-ray CT scans. We can see that X-ray CT scans have been evolved enormously since the first discovery in the early 1970s and it continues today with applications of the artificial intelligence (AI) and deep learning (DL) in our modern CT with promising successful results. In this work, a pedagogical study of our modern X-ray CT with the related review of literature regarding *i-scanning geometry*, *ii-reconstruction techniques,* and *iii-AI&DL applications* is being presented hoping to be useful as a quick reference especially for the scholars and researchers in the field.

Keywords: X-ray computed tomography; X-ray CT; artificial intelligence; deep learning; DL.

1. Introduction

Goal of the computed tomography (CT) is for sure to produce mass-density maps (or maps of X-ray attenuation coefficient distribution as will be explained here soon afterwards) of the internal structure of the 3D objects, i.e., a human body (or parts of the body), as sliced 2D graphs to constitute a 3D CT-scan graph by using directed beams of waves (or rays) through it without cutting or looking from any internal point of it. Ultrasound or X-rays can be used as directed beams through the body to achieve this purpose and we study only the X-ray CT here in this work. As we all are familiar in our modern life today, the CT has become an indispensable tool in our modern medical applications where these produced CT images are frequently used for diagnosis and patient treatment plan by the physicians. Although there is no cut or any means of physical damage to the body under scan to pay for such wonderful images, which also

Artificial Intelligence Theory and Applications, ISSN: 2757-9778. ISBN: 978-605-69730-2-4 © 2023 İzmir Bakırçay University

makes it indispensable in the practical applications of today's health sciences, there is an ALARA (as low as reasonably achievable) principle in medical applications emphasizing as high-quality CT images (with the highest possible resolution) as possible by using as little X-ray exposure of the body under scan as possible [1-9]. To maintain this principle, along with the other demands such as scanning speed, image quality, performance, computational speed, etc., CT scanning technique has been evolved with revolutionary improvement since the first discovery in 1970s [10] and it continuous with the promising applications of today's artificial intelligence (AI) and deep learning (DL) techniques [1,2,4,6-9,11]. This work deals with a brief review of it in a classification and dimensional analyses of the literature regarding the associated principles and techniques in the field.

In this work, we focus on components, development, and literature review of our modern image reconstruction (IR) techniques in the X-ray CT with the conventionally and commercially used analytic image reconstruction (AIR) and iterative image reconstruction (IIR) techniques within the seven-generations of scanning geometries along with the emphasis on recent applications of modern AI and DL in the field. In this work, we shortly study classification of literature in the modern X-ray CT with the dimensional analyses to be as a quick reference guide hoping to be useful for the scholars and the researchers in the field. Main abbreviations for the X-ray CT concept we used in this work (as also conventionally used in the literature) are listed as shown in Table 1.

Table 1. Abbreviations for the X-ray CT concept we used in this work

Name of the category	Name of the category
AI: Artificial intelligence	DLIR-M: Medium-dose DL (applied) image reconstruction
AIR: Analytic image reconstruction	FBP: Filtered back-projection
AR: Analytic (image) reconstruction	IR: Image reconstruction
ART: Algebraic Reconstruction Technique	IIR: Iterative (image) reconstruction
CT: Computer tomography	SART: Simultaneous Algebraic Reconstruction Technique
DL: Deep learning	SIIRT: Simultaneous Iterative Reconstr. Technique (SIIRT)
DLIR: Deep learning (applied) image reconstruction	MLEM: Maximum Likelihood Expectation Maximization
DLIR-H: High-dose DL (applied) image reconstruction	PL: Penalized Likelihood
DLIR-L: Low-dose DL (applied) image reconstruction	

2. Components and development of X-ray CT

From literature, we can say that processes in medical applications of X-ray CT involve the following steps [1,2,4-6,8,9,11-13,16]: i) Scanning the body of the patient by the X-rays and recording the measured intensities of the receding X-rays from the patient (by sensors), which can be called as construction of image data, ii) Acquiring the 2D or 3D graphs of internal structure from scan data, which is called as image reconstruction (IR), and iii) Further image processing of the image reconstructed X-ray CT-scan graphs, such as segmentation, classification, deblurring, etc., which can be called as post IR processing or simply image processing (IP), and iv) Interpreting the image reconstructed CT-scan graphs or post IR-processed graphs by the physicians, i.e., diagnosis, treatment plan, etc., which can be called as clinical (or medical routine) as shown schematically in Fig.1. Artificial Intelligence (AI) and Deep Learning (DL) based parts where we see in IR and post IR-processing steps are marked in red in Fig.1.

We see that major improvement of X-ray CT-scan in history has been in two fields: *i)* in scanning process and *ii)* in IR-process. *Regarding the scanning process*, chronologically we see that there are *seven generations of CT-scans* where design of scanning

apparatus and scanning geometry have been improved with revolutionary designs so far [2,4,10,12,14,15,17-21]. Various scanning geometries are actually the pencil-beam approximation of the early generation X-ray CT scans where discrete scanning angle (θ) and separation of sensors (s) are the two-fundamental parameters forming the dataset of the measured output intensity, in the form, say $I(s,\theta)$, from which the internal mass-density map of the related slice of the body, $f(x,y)$, is formed (*or in CT terms,* reconstructed) [12,14,17,22]. *Regarding the image re-construction process,* since the various scanning geometries are basically the pencil-beam approximated early generation CT-scans, there are basically two fundamental reconstruction techniques inherent from the early generation scans: *i) Analytic image reconstruction (AIR)* [4,23-26] and ii) *iterative image reconstruction (IIR) techniques* [5,24-26]. Note that, IIR methods are sometimes referred to as (or related with) algebraic IR as in [4,12,13,27]. The AIR involving (and also frequently used for AIR interchangeably) the conventional *Filtered back propagation (FBP)* method was the originally used image reconstruction technique used in the early stage of the discovery of the CT-scan through the 1990s and it involves the Fourier-slice theorem where the Fourier transform and reverse Fourier transform are involved with the filtered back-projection (FBP) applications [4,23-26]. Although conventional FBP technique provides theoretically exact solutions assuming noiseless measurement of output X-rays as a line integral of attenuation (ray-sum) through the patient in the IRC process, reconstructed images are normally blurred in practical applications but they can be enhanced by the use of some filters to some extent [4,24-26]. On the other hand, IIR techniques basically rely on the fundamentals of Kaczmarz's algorithm, which was originally proposed by Kaczmarz in 1937 [28], which technically enables better images in greater performance but it could not have found clinical applicability by 2009 at which substantial advances in the hardware technology occurred [13,26].

Most of the recent X-ray CT scans (those without AI and DL applications) use some advanced IR techniques such as Simultaneous Algebraic Reconstruction Technique (SART), Maximum Likelihood Expectation Maximization (MLEM), and Penalized Likelihood (PL), etc., since being in higher performance thanks to the modern advanced hardware technology [5,23,24]. However, the ALARA principle causes restrictions in practical medical (clinical) applications especially in pediatric or other risky applications due to the danger of the exposure of high-dose X-rays for such patients since production of high-quality X-ray CT images require high dose X-ray applications in both AIR and IIR methods [2,17,22]. But this problem seems being solvable through today's advances in the AI and DL fields [1,2,4,6-9,11]. We can see that AI and DL applications to the IRs can provide high quality X-ray CT images with promising results as being used in today's modern X-ray CT scans frequently. We study it in Sect. 5.

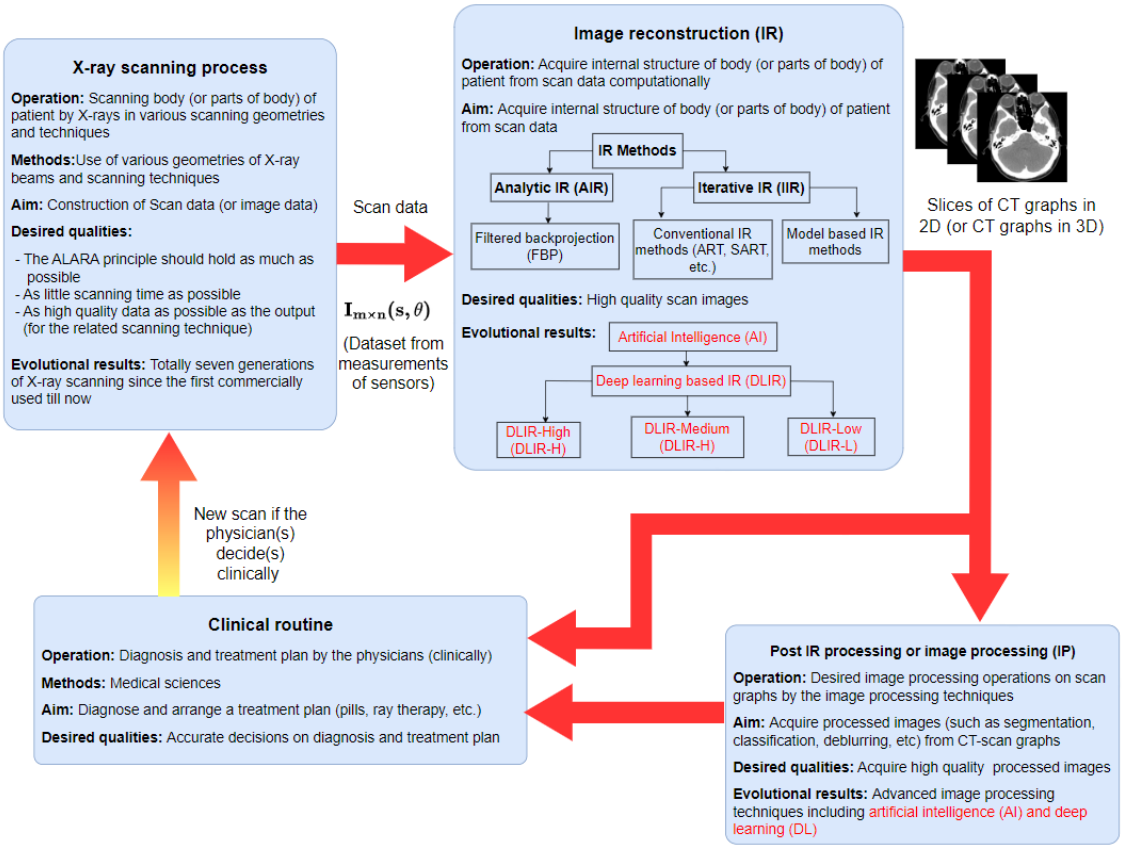

Figure 1. Steps of medical applications of modern X-ray computed tomography

3. Pencil Beam approximation and the Image Reconstruction (IR) Techniques

A schematic sketch of the *"pencil-beam approximated X-ray CT scan"* given in Fig. 1 describes the fundamental model where parallel beams of X-rays are collimated in the form of a so-called *"pencil-beam shape*" where the beams are assumed to be directed from top of a pencil to its tip as an analogy through the patient's body. This model is actually originated from the first-generation scanners which is actually entirely different in comparison to today's scanners where beam shapes (being in fan, conic, etc.) and scanning styles (being in stationary or rotary multi-sensor array in the gantry, helical scan, etc.) are completely different as discussed in the next section. But majority of the scanning techniques can mainly be modelled by this model to explain the fundamental principles of the conventional IR techniques in the X-ray CT [12,14]. We also note that calculations regarding IRs of beam shapes other than pencil-beam approximation are studied in details in [12]. As can be seen from Fig.2, parallel pencil-beam shaped X-rays are very thin (about 1 mm to 10 mm) and they are incident on an outer surface of a 3D object (such as a patient's body or some part of it) to pass through it with an attenuation as a measure of the mass-density distribution of the interior region on the path in the longitudinal direction. The detectors on the other side of the body detect and measure this attenuated output intensities receding from the patient's body when they hit the sensors. Intensities of the parallel input beams (incident on the patient's body) are set to a constant value, say I_0, and the attenuated output beams (from the patient's body) for each scan angle θ is detected and measured by the parallel sensors separated by a distance of s, say $I(s,\theta)$. An entire scan of a slice of a body completes with a total of n numbers of scans between start and end scanning angles θ_1 and θ_n, namely in $\theta_1 \leq$

$\theta_i \leq \theta_n$, as the pairs of sensor and detector arrays attached to the gantry rotates in discreate $\theta \rightarrow \theta_i$ angles as shown in Fig. 1. Since X-rays interact with matter with a longitudinal attenuation depending on the mass-density of the matter at that point via the *Beer-Lambert law* [14,18,23,29-31], measured output intensity of each beam (from the patient's body) is attenuated as a sum of attenuations of each tiny-sliced cubes (or rectangular prisms), called as *voxels (as an implication of three-dimensional pixels)*, in comparison to the input intensity as shown in Fig.1. Consequently, each output beam involves sum of attenuations of each voxel, in other words, sum of mass-density distribution of the body between its end points in the direction of the related X-ray beam through its path. Once a complete scan of a slice is completed for all angles, a 2D graph regarding the measured output intensities for all these scan angles at all the sensor locations, called as a *sinogram,* i.e., [1,12,24]*,* is produced, then the internal structure of the body in the form of mass-density function, say $f(x,z)$, is computationally produced. To illustrate, bones have higher mass-densities hence greater attenuation coefficients in comparison to the fatty regions and a 2D graph of $f(x,z)$ is obviously informative to the physicians showing how the internal structure of the patient's body is.

Fundamental IR techniques, which can be modelled as the pencil-beam approximated model in Fig. 2 as explained above, can be classified conventionally in two groups, namely, analytic image reconstruction (AIR) techniques and iterative image reconstruction (IIR) techniques as being studied in the next sections.

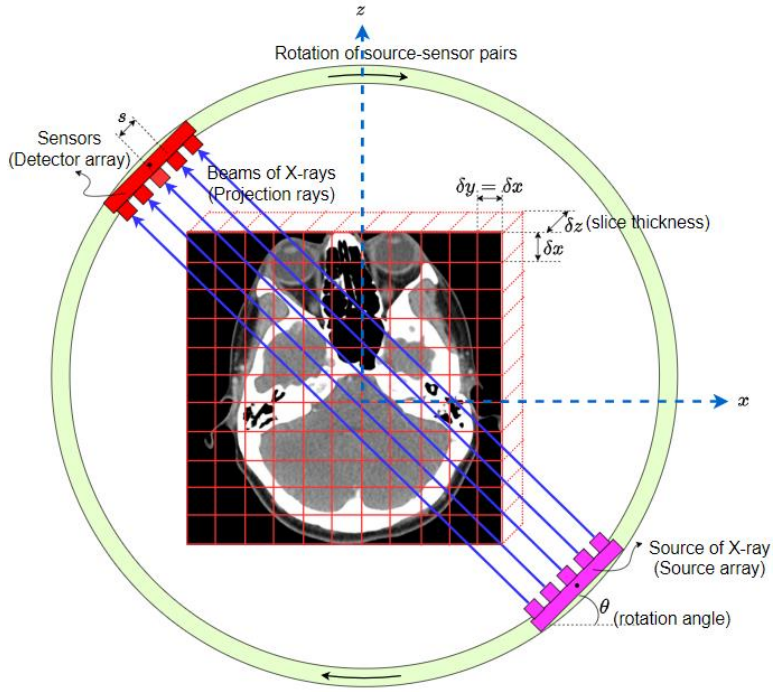

Figure 2. A schematic sketch of pencil-beam approximated X-ray CT-scan.

3.1. A short Review of Analytical Image Reconstruction (AIR) Methods

Most commonly used analytical reconstruction methods on commercial CT scanners are all in the form of filtered back-projection (FBP), which uses a one-dimensional filter on the projection data before back-projecting them onto the image space in 2D [12,17,19,24]. From the conventional pencil-beam approximated model in Fig. 2, we see that both source arrays and the detector arrays (in the opposite side) attached to each

other rotate together in the gantry by an angle of θ for each detector measurement and the process repeats n times in $\theta_1 \leq \theta_i \leq \theta_n$ where i is the index of scan angle (or simply scan index) to complete the whole scan of one slice in total n-scans. Since the intensity of the X-ray detected at the j-th detector (for a specific i −th scan) is attenuated by the longitudinal density of the body under study (along the propagation direction of the X-ray beam), intensities measured by the j −th detector is the line integral of the attenuated intensities (via the Beer-Lambert law) along the path from source to the detector. Another expression involves mathematically a line integral of the mass-density distribution of that region (or voxel) via Dirac Delta function $\delta(xcos\theta_i + zsin\theta_i - s)$ to select the correct path on the line $xcos\theta + zsin\theta$ (See Fig.1), namely,

$$p_i(s,\theta_i) = \int_{-\infty}^{\infty}\int_{-\infty}^{\infty} f(x,z)\delta(xcos\theta_i + zsin\theta_i - s)dxdz. \quad [1]$$

Consequently, projection $p_i(s,\theta)$ represents a line integral whose input is the detector readings for the projection angle $\theta \leftarrow \theta_i$ given in Fig. 2, which is referred to as *mass Radon transform* (or simply Radon transform) [6,12,13,31-33], Now the problem is the inverse process to find $f(x,y)$ from $p_i(s,\theta)$, which is referred to as *inverse Radon transform*. Back projection is not exactly an inverse Radon transform but a kind of a conjugate process to assign a point (x,y) in the object coordinates. Reconstruction process involves the solution of the measured intensity involving measured angle and linear shift position of the related X-ray tube in terms of integral equations by inversion, which is known as the *Back projection*. Traditionally, a filter, called as Ram-Lak filter to compensate the low-pass blur due to the different numbers of projections passing through the center and periphery of the image region is used in the FBP method [6,24,31-33]. FBP involves the Radon transform described above and the Fourier Slice Theorem (FST) which states that the one-dimensional Fourier transform $p(\omega,\theta)$ of a projection $P(s,\theta)$ in parallel-beam geometry for a fixed rotation angle θ is identical to the one-dimensional profile through the origin of the 2-D Fourier transform $F(\omega cos\,\theta, \omega sin\,\theta)$ of the irradiated object element in (x,y).

3.2. A short Review of Iterative Image Reconstruction (IIR) Methods

Conventional IIR methods involve the following: Algebraic Reconstruction Technique (ART), Simultaneous Algebraic Reconstruction Technique (SART), Maximum Likelihood Expectation Maximization (MLEM), Penalized Likelihood (PL), etc. [13,23,30]. In this work, we focus on the ART technique, which is the mostly studied technique originally introduced by Kaczmarz in 1937 for the first time [28]. In the ARTs, related matrix obtained by the detector measurement for various angle scans have an M by N equation system as follows [13, pp.276-278]:

$$W.F = P \Rightarrow \sum_{j=1}^{n} w_{ij}\vec{f}_j = p_i, \;\; s.t.\; i = 1,2,\dots,M; j = 1,2,\dots,N \quad [2]$$

where M is the total number of rays (in all projections), p_i is the ray-sum measured for the i−th ray, w_{ij} is the weighing parameter where Kaczmarz's method is associated. Here value of $f(x,z)$ as a square grid on the related voxel is considered to be constant (since the size of the voxel is too small) and f_j denotes this constant value in the jth cell where N is the total number of cells in the path of the related beam. The problem then becomes finding the unknown $\vec{f}_j$ values from the system of M equations in N unknowns

(where W becomes the matrix of constant coefficients) by the iterative methods as being presented in [13]. To illustrate it, let us suppose a standard 255x255 image, then it means: $N \approx 65.000 \approx M$ with W: MxN matrix (with many zeros due to the voxels not in the beam path). Such a hard work by iterative methods became applicable thanks to the advances in hardware technology around 1990s.

Each linear equation in the system forms a line and the solution is the point of their intersections. Computation starts with an initial guess then it follows its projection firstly on the first line and secondly its projection to the second line to continue the same procedure for all lines. Then it repeats by taking it as the initial guess of the second tour to converge to the intersection point. Finally, it stops when the desired accuracy (or iteration number) has been reached. In each iteration with index i, these guess points have a displacement vector: $\vec{f}^{(i)}$ which is composed of N components: $\vec{f}_1^{(i)}, \vec{f}_2^{(i)}, \ldots, \vec{f}_N^{(i)}$ in the N dimensional space. For example, our initial guess with $\vec{f}^{(0)}$ is firstly projected on the related hyperplane to give $\vec{f}^{(1)}$, then it is projected on the second equation to give $\vec{f}^{(2)}$, and the process continues similarly. In order to get $\vec{f}^{(i)}$ from the $\vec{f}^{(i-1)}$, Kaczmarz's algorithm has the following operation mathematically [13]:

$$\vec{f}^{(i)} = \vec{f}^{(i-1)} - \frac{\left[\vec{f}^{(i-1)}.\vec{w}_i - p_i\right]}{\vec{w}_i.\vec{w}_i}.\vec{w}_i \qquad [3]$$

where $\vec{w}_i = (w_{i1}, w_{i2}, \ldots, w_{iN})$ and $\vec{w}_i.\vec{w}_i$ is the dot product. Proofs and details including the convergence conditions and illustrations for higher dimensions are available in [13,31,34]. Fundamental iterative image reconstruction techniques such as Algebraic Reconstruction Techniques (ART), Simultaneous Iterative Reconstruction Technique (SIIRT), Simultaneous Algebraic Reconstruction Technique (SART), etc. works on this principle.

4. Scanning Geometry and evolution of CT scans

Since the first model of X-ray CT scanner, scanning geometry (and hence scanning mechanism and scanning technology) has been evolved enormously and each revolutionary design has been referred to as a new generation scan. There are totally *seven-generations of X-ray CT-scanners* developed and used so far, all being completely different from each other [2,4,10,12,14,15,17-21]. Although scanning mechanisms could be different, image reconstruction techniques can be studied via the pencil-beam approximated X-ray CT-scan whose schematic sketch is given in Fig.2 since they can be approximated and modelled by it as explained above.

The first and second-generation CT-scanners being of the only translational types among them are as shown schematically in Fig.3. First generation scanner shown Fig.2a has a unique X-ray source and sensor pair and it starts scanning translationally along the x −axis for angle $\theta \to \theta_A = 0°$ in time t as $t_{A0} \le t \le t_{An}$ then angle changes from $\theta_A = 0°$ to θ_B by rotating around the y −axis and the translational scan starts again but in the reverse direction (along the $-x'$ −axis now) in the rotated coordinate system. When it completes, angle then changes from θ_B to θ_C and the translational motion but now being in the reverse direction (along the $+x'$ −axis) in the rotated coordinate system starts again. Consequently, first-generation X-ray CT scanners scan in *"translational-rotational"* modes [10,12,14,18]. Second generation scanner shown Fig.2b has the same *"translational-rotational modes"* like the first generation but it includes many sensors as a sensor array in comparison to the first generation. We see that scanning speed is

increased in the second generation. The first and the second-generation CT scanners are the only scanners having translational scanning modes and no more used in today's medical applications.

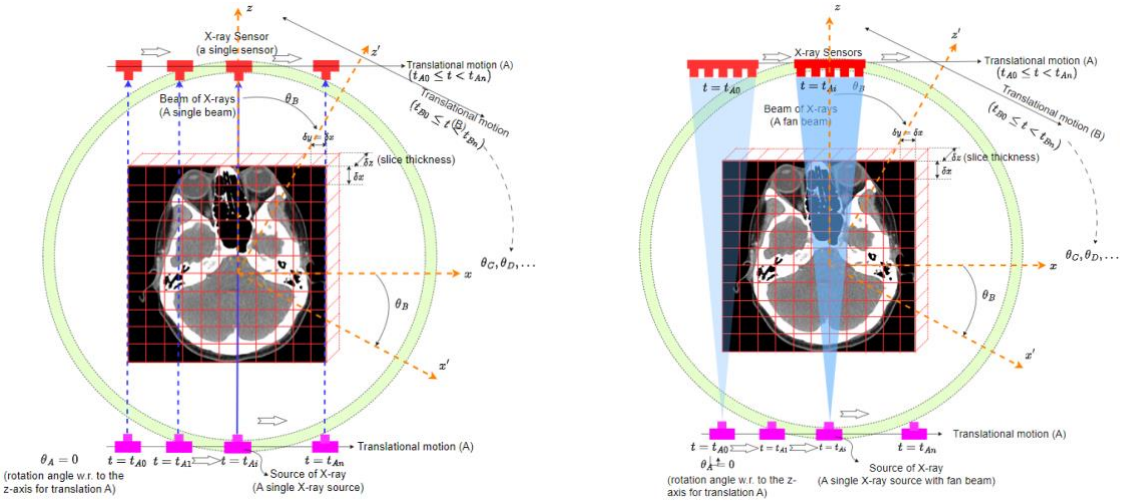

a) First generation b) Second generation

Figure 3. A schematic sketch of the first and second-generation X-ray CT-scanners (not in scale-patient size is exaggerated).

The third and fourth-generation CT-scanners being of the first only-rotary types are as shown schematically in Fig.4. We note here that size of the patient's body (or the organ of the patient under study) in the schematic sketches in Fig. 3&4 are exaggerated with respect to the size of the girth since the beams shown in blue are approximately paraxial (and they would actually fill the entire body if the size of the body were not exaggerated). The third-generation scanner shown in Fig. 4a has a multisensory array attached to a single X-ray source rotates around the y-axis on the gantry. Scanning principle of the fourth-generation CT scanner shown in Fig. 4b is similar to the third generation but the sensor array is stationary and fills the entire inner surface of the gantry [12,18]. The third and fourth-generation CT scanners are the "only rotary mode" scanners (no translational mode).

Several other CT scanning geometries have been developed and marketed afterwards but none of them fits precisely the conventional CT categories studied above. Remaining generations are technologically advanced scanners. Since the scanning time of the first four generations are too long for some certain applications such as cardiac-scans, the fifth generation X-ray CT scanners were developed. They involve an electron beam accelerated by the applied high voltages and deflected by the deflection coils to a stationary tungsten-arc target attached to the inner surface of the gantry running entirely in a *stationary mode* [4,12,14,17]. In the fifth-generation scan, there is no translational or rotational part relative to the gantry, and hence it can be counted as a *"stationary mode"* scanner. As the accelerated and deflected high-energy electrons hit the tungsten arc, X-rays are produced at the point of impact. In other words, the tungsten arc acts as an instantly triggerable X-ray source at the desired position by the high energy electrons. Since the accelerated and deflected electron beams hit the tungsten arc in a very fast rotary scanning nature, scanning speed increases enormously for the applications

requiring high-speed scan like cardiac applications. It is capable of ultra-fast scans, i.e., 50-milisecond scan time and production of 17 CT slices/second, for such special and advanced applications. Its use in cardiac tomographic imaging is frequently referred to as *"cine CT"*.

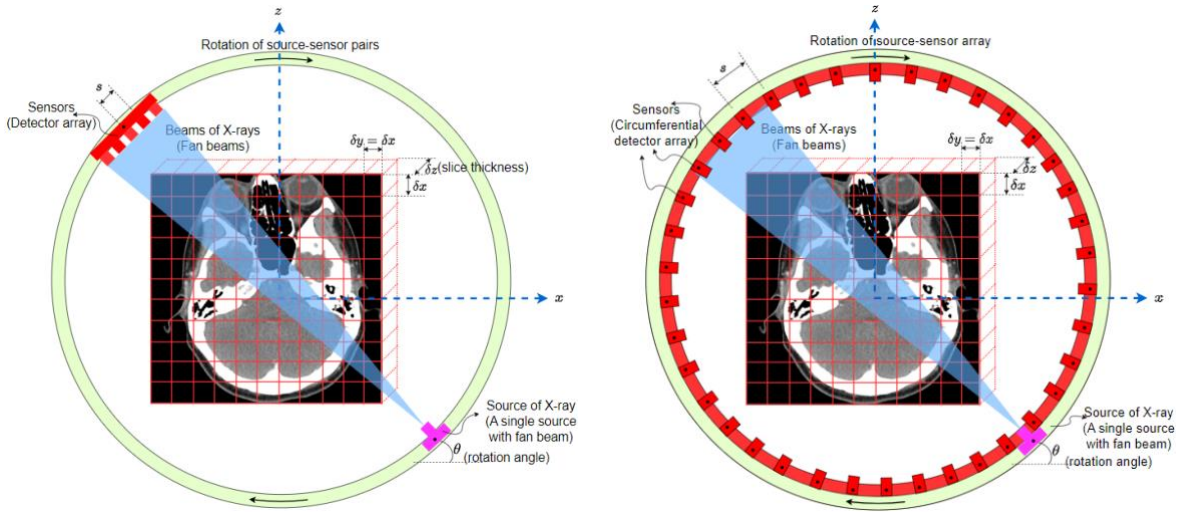

a) Third-generation b) Fourth-generation

Figure 4. A schematic sketch of the third and fourth-generation X-ray CT-scanners (not in scale-patient size is exaggerated).

Although the fifth-generation scanners present much more desired benefits, they are too expensive and consequently, a doughnut-shaped sixth-generation CT scanner was developed. It is frequently referred to as *"spiral/helical CT"* and it involves *"X-ray source rotation"* and *"exam-table translation"* perpendicular to it to form a spiral (or helical) scan around the patient [4,10,12,14,17,18]. In effect, the patient lying on the exam table passes through a doughnut shaped rotating scanner or in other words, x-ray tube rotates in helical path. In conventional scanners, scanning time could be around 10-15 minutes but in some instances, entire scan can take a single breath-hold time in the 6th generation CTs. It is also called as *"volumetric scanners"* since having a single fan-beam source and a stationary multidetector array in the gantry to fill a volume of X-rayed tissue. It provides high image resolution and improved image quality. Due to the helical path, a three-dimensional data set is obtained and they are used for image reconstruction into sequential images for a stack. In the sixth generation, the tube is energized continuously, and data are also collected continuously. The gantry also rotates continuously. It involves a slip-ring technology and there are three slip-rings attached to the gantry as terminal connections to the X-ray tube, detector and control sensors which enables a high-speed rotation. Slip-ring arrangement enables a rotation speed around 5s/rot a rotation angle more than 360° as a continuous rotation with continuous data acquisition. As to the seventh-generation scanners, it involves multi-sliced detectors allowing acquisition of multiple slices in single row and this makes it to be frequently referred to as *"MS (multi-slice) CT-scanners"* [2,14,17,19]. They are the most advanced X-ray scanners developed so far. It generally uses third generation CT shown in Fig.4a with helical scanning and low voltage slip rings. In the seventh generation CTs, A body section can be scanned faster with a multiple row of detectors system with multiple fan beams scanning simultaneously. It also uses slip-ring technology for switching power and image

data. It involves a conical shaped fan-beam and a fast rotation speed (about 0.5 to 0.8 sec per rotation) which reduces the examination time. The image quality is mostly similar to that of single slice scanners. It enables high spatial resolution.

5. Artificial Intelligence (AI) and Deep Learning (DL) in X-ray CT

We have seen that scan techniques (or geometries) and IR techniques in X-ray CT have evolved to maintain the ALARA principle to produce CT images in high qualities besides other needs such as high performance, high scan and IR speed, etc. Now we continue with that application of AI and DL in the IR stage, as marked in red in Fig. 1, being *closely related to the scan technique and the IR techniques* we studied above, can give promising results. We will also see that, beside the IR stage, AI and DL can also be applied as post-IR applications for some specific purposes of image processing, like segmentation, classification, deblurring, etc. as their classical uses to maintain clinical needs. In X-ray CT, any result which might seem perfect in X-ray CT graphs should also be tested and studied clinically [1,35]. Hence, we also review the related articles in this section.

DL is actually a sub-class of the Machine learning (ML) which is also a sub-class of the AI as shown in Fig. 5 [1,35]. The Artificial neural networks (ANNs) are one of the methods in the ML and Deep neural networks (DNN) are some special types and more advanced form of the ANNs. DNNs involve the Convolutional neural networks (CNNs) which involves advanced network architecture and their principles are available in [1,11,35] as well as ordinary conventional AI/DL textbooks.

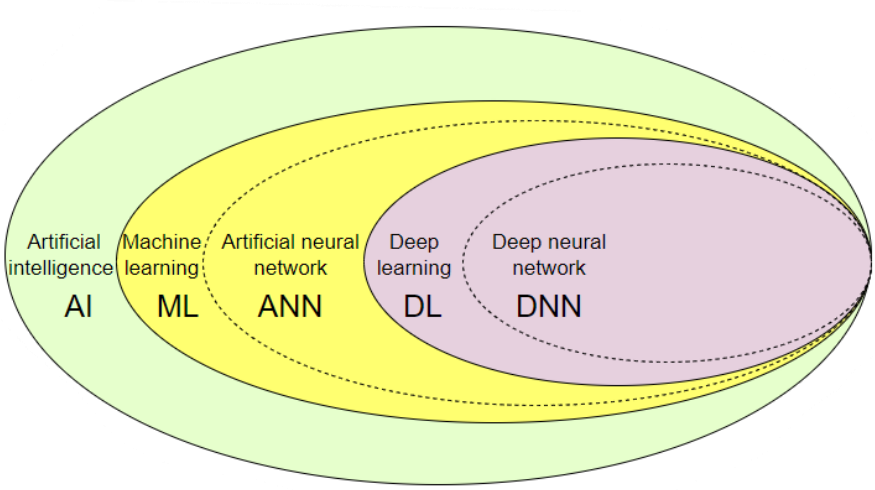

Figure 5. Schematic sketch of clusters of Artificial intelligence

We have seen above that IR techniques of most of the scan geometries (for all seven-generations of CT-scans) can be studied in the conventional Pencil-beam approximated model where the sensor readings in eqn. (1) are $p_i(s,\theta_i)$ for the i −th scan index in a single slice-scan. Then the IR part works out to reconstruct the mass-density function (or the X-ray attenuation function of the body) by computing function f in (1) or (2) analytically (for the AIR) or iteratively (for the IIR). From literature we know that the FBP, which is the conventional and fundamental of the AIR methods, gives better results than the IIR methods when it is used with the necessary filters (also including the AI/DL applications as filters), though IIR enables advanced modifications for greater performance [1,5,7,8,11,20,22,36-38] *(See also Fig. 5)*. However, there is a serious

problem that the superior FBP method (with respect to the IIR techniques) requires application of high-dose X-ray beams to the body under scan for higher image qualities, which violates the ALARA principle [5,7,8,11,36]. This problem and the solution suggested by one of the vendors of AI/DL-based CT-scan systems (GE Healthcare) regarding the effect of the application of AI/DL to the IR process is shown in Fig. 6 [36].

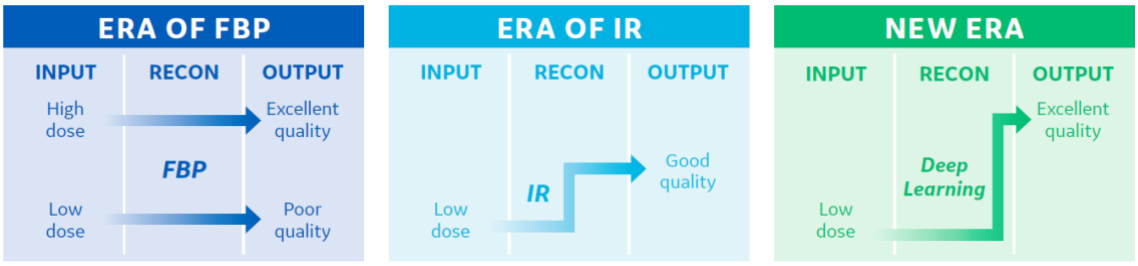

Figure 6. Comparison of the constructed image results of AIR (or FBP) and IIR techniques with the so-called new area, that is, AI/DL-applied IR (image reconstruction) [36]).

Today, we see from literature that success of the AI and DL applied X-ray CT are being tested and reported in various medical applications, such as scans in pediatry, brain-trauma, lung, etc., in the health sciences, i.e., [1,38-54]. Such practical applications involve commercially available in three forms: *high*-dose deep learning (based) image reconstruction (DLIR-H), *medium*-dose deep learning (based) image reconstruction (DLIR-M), and *low*-dose deep learning (based) image reconstruction (LDLIR-H) modules commercially available by two vendors (to our knowledge), namely, TrueFidelity by GE Healthcare and AiCE by Canon Medical Systems [1,35-54]. Mechanism of AI/DL applied X-ray CT given in [36,39] relies on using FBP-reconstructed high-quality images (obtained by high-dose X-ray application) as *ground truth images* in supervised learning. Here, ground truth images are the images of our training dataset used in the related DNN designed [1]. Some of the clinical results of AI/DL-based X-ray CT work with apparently promising results are given in Table 2 where Image qualities obtained after the reconstruction techniques under study (AI/DL-applied or other classical IRs) are evaluated and compared with each other by either qualitatively, or quantitatively, such as in [38,41,46]. In these papers, as being standard routine, qualitative evaluations and comparisons are made by the experienced physicians contrary to the conventional quantitative work in the field of image processing where image parameters such as Signal to noise ratio (SNR) and Contrast to noise ratio (CNR) are evaluated and compared [1,2,11].

Table 2. Dimensional analyses of some AI/DL based clinical CT applications by GE Healthcare's TrueFidelity™.

Ref. #	Organ, CT type, experimental (phantom, patient, etc.)	Feature and/or aim of the work	Properties and outcomes
[38]	Head CT in trauma	Image optimization	DLIR outperformed ASIR-V both qualitatively and quantitatively
[39]	Pediatric, head CT	-Image optimization: *improve image quality* -Detection: *lesion detection*	DL-H reduces noise and improves quality of the images
[40]	Chest CT (with aorta, lung tissue, subscapularis muscle, liver, and vertebrae), 50 patients but 48 selected (22 male, 26 female)	Image optimization: *Comparison of SNR and CNR values obtained by DLIR-M, DLIR-H, and ASIR-V 50% by ANOVA (or the Friedman) test*	-All three IRs do not change significantly for $p<0.001$ but differ in soft tissue for $p>0.05$. -Order of best noise reduction (by increasing CNR and CNR) without

[41]	Abdominal CT, 50 patients (62%F; 56.74∓17.05 years)	Image optimization: *Comparison of image quality of IRs obtained by ASIR-V at 40%, DLIR-L, DLIR-M, and DLIR-H qualitatively and quantitatively (200 datasets, each IR technique being 50 data).* *-Qualitative analyses: by a point-based Likert scale adapted from the European guidelines on quality criteria for CT.* *-Quantitative analyses: by CNR for portal vein and liver via ANOVA (or the Friedman test).*	distorting the image texture: DLIR-H>DLIR-M>ASIR-V% → Qualitatively: -DLIRs had better absolute scores than ASIR-V. -DLIR-H demonstrated the best image quality performance compared to ASIR-V for all metrics. - Figure of merit (FOM) analysis also demonstrated that qualitative improvements were amplified by the DLIR →Quantitatively: - All DLIRs had better qualitative scores than ASIR-V. -Compared to ASIR-V, DLIRs had a lower image noise (2.86 vs 1.40–2.29), better image contrast (2.55 vs 1.41–1.96), finer small structure visibility (2.34 vs 1.51–1.90), and improved image sharpness (2.01 vs 1.60–1.86). -Among DLIRs, DLIR-H had the best scores followed by DLIR-M and DLIR-L. -Mean time to reconstruct images with DLIR was longer than with ASIR-V.
[45]	Phantom study with 7 dose levels: $CTDI_{vol}$: 15/10/7.5/5/2.5/1/0.5mGy	Image optimization: *Comparison of image quality of FBP, ASİR-V50%(AV50), ASİR-V100%(AV100), DLIR-L, DLIR-M, and DLIR-H via noise-power spectrum (NPS) and task-based transfer function (TTF)*	The new TrueFidelity™ deep learning image reconstruction algorithm reduced noise magnitude and improved spatial resolution and detectability without changing noise texture relative to FBP.

6. Conclusion and Discussion

In this work, we have studied a general review of X-ray CT focusing on scanning technique (or scan geometry) and IR techniques along with their relationship with the ALARA principle pedagogically. We see that, regarding the scan geometry, there are seven generations of CT-scans so far and two-main types of image reconstruction techniques: i) Analytical image reconstruction (AIR) and ii) Iterative image reconstruction (IIR). Here we have shortly reviewed the main principles about IR and CT-scanning techniques with the application of AI/DL via the considerations of the ALARA principle. We see that clinical results show promising results for the application of AI/DL in X-ray CT applications. We hope that this work becomes useful as a quick and brief reference for the scholars and researches in the field of AI/DL and X-ray CT.

References

[1] Arndt, C. et al. (2021). Deep Learning CT Image Reconstruction in Clinical Practice. Fortschr Röntgenstr, (193), 252–261.

[2] Booij, R., et al. (2020). Technological developments of X-ray computed tomography over half a century: User's influence on protocol optimization. European Journal of Radiology, (131), 109261.

[3] Bueno et al. (2018). Development of a New Cone-Beam Computed Tomography Software for Endodontic Diagnosis. Brazilian Dental Journal, 29(6). 517-529. http://dx.doi.org/10.1590/0103-6440201802455.

[4] Liu, Y. (2018). Ch. 5: Research Status and Prospect for CT Imaging of book: "State of the Art in Nanobioimaging". IntechOpen, 73-93. https://www.intechopen.com/chapters/58660.

[5] Padole, A., Khawaja, R., D., A., Kalra, M., K., Singh, S. (2015). CT Radiation Dose and Iterative Reconstruction Techniques, Residents' Section-Structured Review, AJR, (204), W384–W392.

[6] Samei, E. & Pelc, N. (2020). Computed Tomography Approaches, Applications, and Operations: Approaches, Applications, and Operations. Springer Nature, 2020, Switzerland. Doi: 10.1007/978-3-030-26957-9 (e-book).

[7] Xing, R. (2020). Deep Learning Based CT Image Reconstruction, MSc Thesis, University of Washington.

[8] Sun J, Li H, Wang B, Li J, Li M, Zhou Z, Peng Y. (2021). Application of a deep learning image reconstruction (DLIR) algorithm in head CT imaging for children to improve image quality and lesion detection. BMC Med Imaging, 21(1), 108. doi: 10.1186/s12880-021-00637-w. PMID: 34238229; PMCID: PMC8268450.

[9] Zhong J, Wang L, Shen H, Li J, Lu W, Shi X, Xing Y, Hu Y, Ge X, Ding D, Yan F, Du L, Yao W, Zhang H. (2023). Improving lesion conspicuity in abdominal dual-energy CT with deep learning image reconstruction: a prospective study with five readers. Eur Radiol., doi: 10.1007/s00330-023-09556-6. Epub ahead of print. PMID: 36976337.

[10] Kalender, W. A. (2006). X-ray computed tomography, Phys. Med. Biol., 51, R29–R43.

[11] Lee T, Seeram E. (2020). The use of artificial intelligence in computed tomography image reconstruction: A systematic review. Radiol Open J., 4(2): 30-38. doi: 10.17140/ROJ-4-129.

[12] Buzug, T., M. (2008). Computed Tomography: from Photon Statistics to Modern Cone-Beam CT, Springer, Berlin, Heidelberg.

[13] Kak, C., A., Slany, M., Principles of computerized tomographic imaging, IEEE press, 1999.

[14] Michael, G. (2001). X-ray computed tomography, Phys. Educ., 442-451.

[15] Romans, L., E. (2019). Computed tomography for technologists: A comprehensive text, 2nd ed., Wolters Kluwer.

[16] Venkatesh, E., Elluru, S., V.(2017). Cone beam computed tomography: basics and applications in dentistry, J Istanbul Univ Fac Dent., 51 (3 Suppl 1), S102-S121.

[17] Cunningham, I. A., Philip, F. J.. (2000). Computed Tomography, CRC Press LLC.

[18] Ginat, D. T., Gupta, R. (2014). Advances in Computed Tomography Imaging Technology, Annu. Rev. Biomed. Eng., 16, 431–453.

[19] Goldman, L., W. (2007). Principles of CT and CT Technology, J Nucl Med Technol., 35, 115–128. DOI: 10.2967/jnmt.107.042978.

[20] Lell, M. M, Wildberger, J. E., Alkadhi, H., Damilakis, J., Kachelriess, M. (2015). Evolution in computed tomography: the battle for speed and dose. Investigative Radiology, 50(9), 629-644. DOI: https://doi.org/10.1097/RLI.0000000000000172.

[21] Akagi, M., Nakamura, Y., et al. 2019. Deep learning reconstruction improves image quality of abdominal ultra-high-resolution CT. Eur Radiol, 29(11), 6163–6171. (Erratum in: Eur Radiol. 2019 May 27, PMID: 30976831).

[22] Hsieh, J., Nett, B., Yu, Z. et al. (2013). Recent Advances in CT Image Reconstruction. Curr Radiol Rep, 1, 39–51. https://doi.org/10.1007/s40134-012-0003-7

[23] Assili, S. (17 Sep 2018). A Review of Tomographic Reconstruction Techniques for Computed Tomography, arXiv:1808.09172v2 [physics.med-ph], 1-5.

[24] Geyer, L., L., Schoepf, U., J., et al. (2015). State of the Art: Iterative CT Reconstruction Techniques, Radiology. 276(2), 339-357.

[25] Ji, D., Qu, G., Liu, B. (2016). Simultaneous algebraic reconstruction technique based on guided image filtering, Optics Express, 24(14), 15897-15911.

[26] Willemink, M. J., Noel, P. B. (2019). The evolution of image reconstruction for CT—from filtered back projection to artificial intelligence, Computed Tomography, European Radiology, 29, 2185–2195. https://doi.org/10.1007/s00330-018-5810-7.

[27] Rubin, G. D. (2014). Computed Tomography: Revolutionizing the Practice of Medicine for 40 Years, Radiology, 273(2 Suppl.), (Suppl), 545-74. doi: 10.1148/radiol.14141356. PMID: 25340438.

[28] Kaczmarz, S. (1937). Angenäherte auflösung von systemen linearer Gleichungen, Bull. Int. Acad. Sci. Pologne, 35, 355–357.

[29] Yusoff, M. S. M., Sulaiman R., Shafinah, K.. (2012). Image Reconstruction for CT Scanner by Using Filtered Back projection Approach, Journal of American Science; 8(6), 797-803.

[30] Jorgensen, J. S. (2013). Sparse Image Reconstruction in computed tomography, Technical University of Denmark PHD-2013 No. 293.

[31] Kharfi, F. (2013). Ch. 4: Mathematics and Physics of Computed Tomography (CT): Demonstrations and Practical Examples of book: “Imaging and Radioanalytical Techniques in Interdisciplinary Research”, IntechOpen, 81-106.

[32] Onur, T., Ö. (2021). An application of filtered back projection method for computed tomography images, International Review of Applied Sciences and Engineering, 12, (2), 194-200.

[33] Siahaan, F. M. (2008). Computed Tomography (CT) image reconstruction using Matlab programming, Master thesis in University of Indonesia.

[34] Golsher, J., G. (1977). Iterative Three-Dimensional Image Reconstruction from Tomographic Projections. Computer Graphics and Image Processing, 6, 513-537.

[35] Do S, Song KD, Chung JW. (2020). Basics of Deep Learning: A Radiologist's Guide to Understanding Published Radiology Articles on Deep Learning. Korean J Radiol., 21(1), 33-41. https://doi.org/10.3348/kjr.2019.0312

[36] Hsieh, J., et al. (2019). A new era of image reconstruction: True Fidelity, Technical white paper on deep learning image reconstruction. www.gehealthcare.com.

[37] Kim, Y., et al. (2015). Ultra-Low-Dose CT of the Thorax Using Iterative Reconstruction: Evaluation of Image Quality and Radiation Dose Reduction. AJR, 204, 1197-1202.

[38] Alagic, Z., Diaz Cardenas, J., Halldorsson, K. et al. (2022). Deep learning versus iterative image reconstruction algorithm for head CT in trauma. Emerg Radiol, 29, 339–352. https://doi.org/10.1007/s10140-021-02012-2, https://doi.org/10.1007/s10140-021-02012-2

[39] Dominik, C., B., et al. (2020). Validation of deep-learning image reconstruction for coronary computed tomography angiography: Impact on noise, image quality and diagnostic accuracy, 14(5), 444-451.

[40] Jiang, J-M., Miao, L., Liang, X., Liu, Z-H., Zhang, L., Li, M. (2022). The Value of Deep Learning Image Reconstruction in Improving the Quality of Low-Dose Chest CT Images. Diagnostics, 12(10), 2560. https://doi.org/10.3390/diagnostics12102560.

[41] Parakh, A., Cao, J., Pierce, T., T. et al. (2021). Sinogram-based deep learning image reconstruction technique in abdominal CT: image quality considerations. Eur Radiol, 31, 8342–8353. https://doi.org/10.1007/s00330-021-07952-4

[42] Bie, Y., Yang, S., Li, X., Zhao, K., Zhang, C., Zhong, H. (2022). Impact of deep learning-based image reconstruction on image quality compared with adaptive statistical iterative reconstruction-Veo in renal and adrenal computed tomography. J Xray Sci Technol., 30(3), 409-418. doi: 10.3233/XST-211105. PMID: 35124575; PMCID: PMC9108564.

[43] Kim, J., H., Yoon, H., J., Lee, E., Kim, I., Cha, Y., K., Bak, S., H. (2021). Validation of Deep-Learning Image Reconstruction for Low-Dose Chest Computed Tomography Scan: Emphasis on Image Quality and Noise. Korean J Radiol., 22(1), 131-138. doi: 10.3348/kjr.2020.0116. Epub 2020 Jul 27. PMID: 32729277; PMCID: PMC7772377.

[44] Tian, Q., Li, X., Li, J., Cheng, Y., Niu, X., Zhu, S., Xu, W., Guo, J. (2022). Image quality improvement in low-dose chest CT with deep learning image reconstruction. J Appl Clin Med Phys., 23(12), e13796. doi: 10.1002/acm2.13796. Epub 2022 Oct 9. PMID: 36210060; PMCID: PMC9797160.

[45] Greffier, J., Hamard, A., Pereira, F., Barrau, C., Pasquier, H., Beregi, J.,P., Frandon, J. (2020). Image quality and dose reduction opportunity of deep learning image reconstruction algorithm for CT: a phantom study. Eur Radiol., 30(7), 3951-3959. doi: 10.1007/s00330-020-06724-w. Epub 2020 Feb 25. PMID: 3210009.

[46] Jiang, C., Jin, D., Liu, Z. et al. (2022). Deep learning image reconstruction algorithm for carotid dual-energy computed tomography angiography: evaluation of image quality and diagnostic performance. Insights Imaging, 13, 182. https://doi.org/10.1186/s13244-022-01308-2.

[47] Noda, Y., Iritani, Y., Kawai, N. et al. (2021). Deep learning image reconstruction for pancreatic low-dose computed tomography: comparison with hybrid iterative reconstruction. Abdom Radiol, 46, 4238–4244. https://doi.org/10.1007/s00261-021-03111-x.

[48] Sun, J., Li, H., Wang, B., Li, J., Li, M., Zhou, Z., Peng, Y. (2021). Application of a deep learning image reconstruction (DLIR) algorithm in head CT imaging for children to improve image quality and lesion detection. BMC Med Imaging. 21(1), 108. doi: 10.1186/s12880-021-00637-w. PMID: 34238229; PMCID: PMC8268450.

[49] Sun, J,, Li. H., Li, H., Li, M., Gao, Y., Zhou, Z., Peng, Y. (2022). Application of deep learning image reconstruction algorithm to improve image quality in CT angiography of children with Takayasu arteritis. J Xray Sci Technol, 30(1), 177-184. doi: 10.3233/XST-211033. PMID: 34806646.

[50] Yoo, Y., J., Choi, I., Y., Yeom, S., K., Cha, S., H., Jung, Y., Han, H. J., Shim, E. (2022). Evaluation of Abdominal CT Obtained Using a Deep Learning-Based Image Reconstruction Engine Compared with CT Using Adaptive Statistical Iterative Reconstruction. J Belg Soc Radiol, 106(1), 15. doi: 10.5334/jbsr.2638. PMID: 35480337; PMCID: PMC8992765.

[51] Li, Y., Jiang, Y., Yu, X., Ren, B., Wang, C., Chen, S., Ma, D., Su, D., Liu, H., Ren, X., Yang, X., Gao, J., Wu, Y. (2022). Deep-learning image reconstruction for image quality evaluation and accurate bone mineral density measurement on quantitative CT: A phantom-patient study. Front Endocrinol (Lausanne). 13, 884306. doi: 10.3389/fendo.2022.884306. PMID: 36034436; PMCID: PMC9403270.

[52] Nakamura, Y., Higaki, T., et al. (2019). Deep Learning–based CT Image Reconstruction: Initial Evaluation Targeting Hypovascular Hepatic Metastases. Radiology: Artificial Intelligence, 1, e180011.

[53] Higaki, T., Nakamura, Y., Zhou, J., et al. (2020). Deep Learning Reconstruction at CT: Phantom Study of the Image Characteristics. Academic Radiology, 27, 82–87.

[54] Narita, K., Nakamura, Y., Higaki, T., et al. (2020). Deep learning reconstruction of drip-infusion cholangiography acquired with ultra-high-resolution computed tomography. Abdom Radiol., 45, 2698–2704. http://link.springer.com/10.1007/s00261-020-02508-4